(12)

EDGEWOOD RESEARCH, DEVELOPMENT & ENGINEERING CENTER

ERDEC-TR-106

MIRROR VELOCITY SAMPLING ERRORS IN A MICHELSON INTERFEROMETER

R.J. Combs
R.B. Knapp

RESEARCH AND TECHNOLOGY DIRECTORATE

P.E. Field

VIRGINIA POLYTECHNICAL INSTITUTE AND STATE UNIVERSITY

Blacksburg, VA 24601-0219

September 1993

U.S. ARMY CHEMICAL AND BIOLOGICAL DEFENSE AGENCY

Aberdeen Proving Ground, Maryland 21010-5

Disclaimer

The findings in this report are not to be construed as an official Department of the Army position unless so designated by other authorizing documents.

REPORT DOCUMENTATION PAGE

Form Approved
OMB No 0704-0188

1. AGENCY USE ONLY (Leave blank)	2. REPORT DATE	3. REPORT TYPE AND DATES COVERED
	1993 September	Final, 92 Jun - 93 May

4. TITLE AND SUBTITLE
Mirror Velocity Sampling Errors in a Michelson Interferometer

5. FUNDING NUMBERS
TA-DARPA A0-8304

6. AUTHOR(S)
Combs, R.J., Knapp, R.B. (ERDEC); and
Field, P.E. (Virginia Polytechnical Institute and State University)

7. PERFORMING ORGANIZATION NAME(S) AND ADDRESS(ES)
DIR, ERDEC,* ATTN: SCBRD-RTM,
APG, MD 21010-5423
Virginia Polytechnical Institute and State University, Department of Chemistry,
Blacksburg, VA 24601-0219

8. PERFORMING ORGANIZATION REPORT NUMBER
ERDEC-TR-106

9. SPONSORING / MONITORING AGENCY NAME(S) AND ADDRESS(ES)

10. SPONSORING / MONITORING AGENCY REPORT NUMBER

11. SUPPLEMENTARY NOTES
*When this study was conducted, ERDEC was known as the U.S. Army Chemical Research, Development and Engineering Center, and the ERDEC authors were assigned to the Research Directorate.

12a. DISTRIBUTION / AVAILABILITY STATEMENT
Approved for public release; distribution is unlimited.

12b. DISTRIBUTION CODE

13. ABSTRACT (Maximum 200 words)

Mirror velocity variations in a continuous mirror drive Michelson interferometer result in erroneous interferogram sampling. The effects of systematic and random mirror fluctuations are evaluated. Four methods of evaluation provide a means to quantify the importance of mirror velocity errors in the Fourier spectrometer's performance as a spectroradiometer. The four methods are time interval signal analysis, sine wave test, optical chopper modulation, and examination of consecutive interferograms. Examination of consecutive interferograms includes the monitoring of a constant blackbody infrared radiation source as well as an interposed ammonia sample cell for wavenumber axis registration. Each method furnishes a known input to the interferometer modulation equation (i.e., 2tm = f) and permits an internal validation of the interferometer mirror velocity evaluation results.

14. SUBJECT TERMS
Time interval analysis
Michelson interferometry
Infrared Fourier transform spectrometry

15. NUMBER OF PAGES
44

16. PRICE CODE

17. SECURITY CLASSIFICATION OF REPORT	18. SECURITY CLASSIFICATION OF THIS PAGE	19. SECURITY CLASSIFICATION OF ABSTRACT	20. LIMITATION OF ABSTRACT
UNCLASSIFIED	UNCLASSIFIED	UNCLASSIFIED	UL

Blank

PREFACE

The work described in this report was authorized under Task No. DARPA AO-8304. This work was started in June 1992 and completed in May 1993.

The use of trade names or manufacturers' names in this report does not constitute an official endorsement of any commercial products. This report may not be cited for purposes of advertisement.

This report has been approved for release to the public. Registered users should request additional copies from the Defense Technical Information Center; unregistered users should direct such requests to the National Technical Information Service.

Acknowledgments

The author would like to thank Gerald Auth (MIDAC Incorporated, Irvine, CA) for helpful suggestions and detailed electronic information necessary to perform this investigation with the MIDAC emission spectrometer.

Blank

CONTENTS

LIST OF FIGURES

List of Tables

MIRROR VELOCITY SAMPLING ERRORS IN A MICHELSON INTERFEROMETER

1. INTRODUCTION

The proper operation of a Fourier transform spectrometer, using a Michelson interferometer, requires uniform sampling of the interferogram along the optical path difference (OPD) scale. Various models and experiments identify nonuniform sampling along the OPD scale as a major source of error for Fourier transform spectrometers.[1-4]

This investigation focuses on four practical methods to determine the accuracy and precision necessary in maintaining a constant mirror velocity (i.e., uniform sampling intervals along the interferometer OPD scale). The four methods (see Figure 1) provide complementary and supplementary information on the effects of interferometer mirror velocity fluctuations. The first method, time interval analysis, measures the dynamic variation of the digitized Helium Neon (HeNe) laser reference signal from the interferometer.[5] The second method, a sine wave test, replaces the preamplifier input signal with a well characterized sinusoidal input. This sinusoidal input simulates a variety of conditions difficult to achieve experimentally.[6] The third method, a chopper modulation of an extended blackbody radiation source, permits the optical generation of a sinusoidal signal that compares directly to the results of the sine wave test. The fourth and final method, examination of consecutive interferograms in either the time or frequency domain, allows the determination of the spectrometer precision.[4,7] The results from these methods supply a means to quantify the importance of mirror velocity errors in the Fourier transform spectrometer performance as a spectroradiometer.[8]

This study examines two spectrometer configurations in the interferometer mirror servo control loop, Cases A and B. In Case A, interferogram sampling near the moving interferometer mirror turn around causes a large systematic acceleration error. In Case B, interferogram sampling is delayed until the moving interferometer mirror attains a nearly constant velocity. The delayed interferogram sampling avoids the acceleration effects of the interferometer mirror turn around. The four methods evaluating the interferometer moving mirror fluctuations permit a diagnosis of an incorrect Case A mirror servo control configuration. Confirmation of Case B operation with the proper mirror servo control insures spectrometer data collection with minimal sampling errors. The use of synthetic mirror servo control signals for the sine wave test furnishes an idealized instance of no mirror velocity sampling errors (Case C). The operational Case B compared to the idealized Case C for the sine wave test demonstrates that the mirror velocity sampling errors in Case B are indeed minimal.

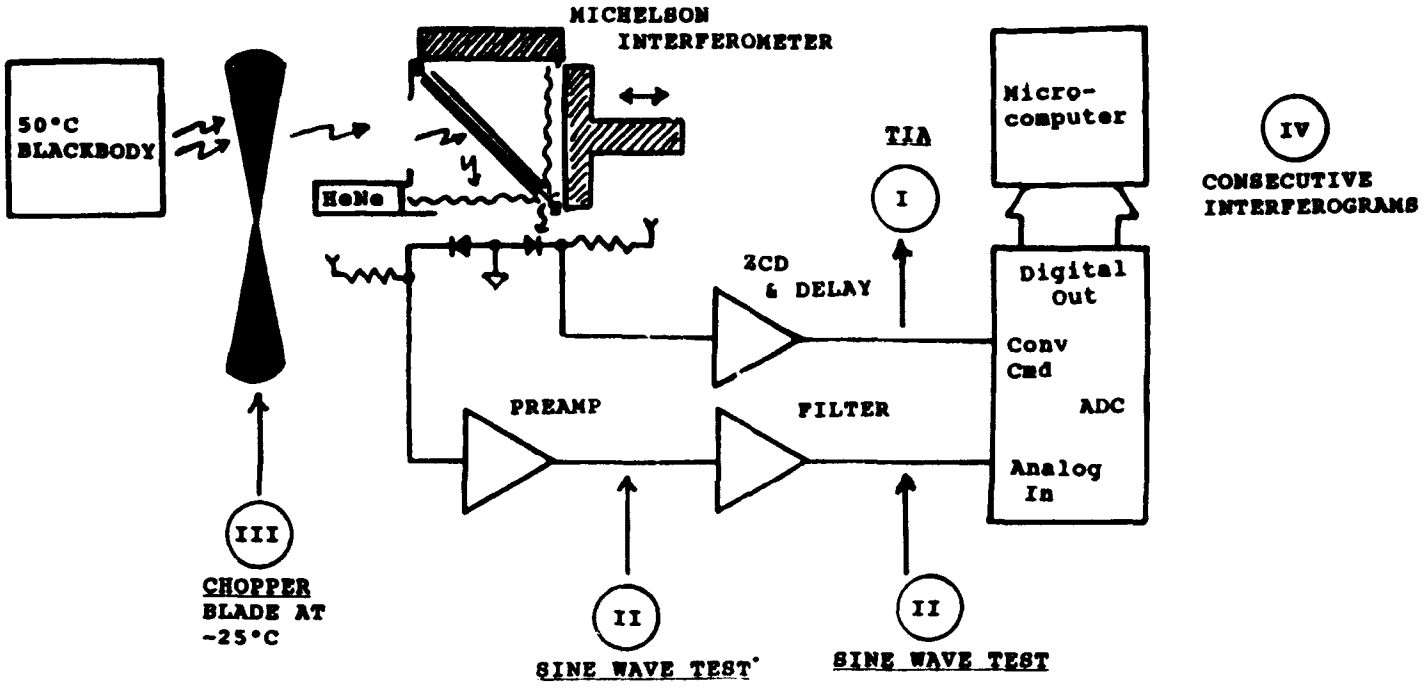

Figure 1. Four Mirror Velocity Error Measurements: I. Time Interval Analysis; II. Sine Wave Test; III. Chopper Modulation; and IV. Consecutive Interferograms

2. EXPERIMENTAL METHODS

The four methods determining the interferometer mirror velocity implement each of the following resources. The MIDAC Outfielder M2400-ZnSe spectrometer Unit 120 (MIDAC, Incorporated, Irvine, CA) contains a 60° field-of-view and 2 mm^2 liquid nitrogen cooled Hg:Cd:Te detector [Judson Model J15D14-M227-S02M-60 (Judson Infrared, Incorporated, Montgomeryville, PA), serial number 20506]. The spectrometer provides 1024 point interferograms at 4 cm^{-1} resolution. A version of the program MIDCOL permits data collection of consecutive interferograms.* The commercially available Spectra Calc software (Galactic Industries Corporation, Salem, NH) allows data analysis of the interferometric data.[9]

The time interval analysis (TIA) of the digitized HeNe laser reference signal (DLR) uses the instrumental techniques described previously.[5] To perform the TIA on the DLR signal from the MIDAC spectrometer for Case B (i.e., only small sinusoidal mirror velocity fluctuations) requires discarding approximately 400 interferogram points (i.e., 800 time intervals) preceding the interferogram centerburst. A block diagram in Figure 2 shows the necessary circuit functions that result in the delay of the signal status (SSTAT) signal [i.e., delayed status (DSTAT)]. The switch inputs to the digital magnitude comparator determine the number of interferogram points by which SSTAT is delayed. This delay before initiation of interferogram sampling (i.e., discarding points) removes the large systematic acceleration error otherwise present when sampling near the interferometer mirror turn around. The timing diagram in Figure 3 indicates the sequence of events that occur in generation of DSTAT. If this SSTAT signal is a digital low, then the counter in Figure 2 is continuously reset. An active digital high on SSTAT enables the counter to begin counting the DLR pulses. The counting of the DLR pulses continues until the counter output matches the switch settings (i.e., 416 decimal). The digital comparator for equal inputs of counter and switches produces an active digital high output pulse on the A = B output. The digital comparator A = B output pulse sets the reset-set (RS) flip flop and enables DSTAT. The DSTAT remains enabled until reset by SSTAT, then becoming an inactive digital low.

The sine wave test replaces the infrared (IR) preamplifier signal with a 1 V peak-to-peak, 500 Hz sine wave.[6] The Analogic 2020 polynomial waveform synthesizer (PWS)[10] generates the input sine wave for the spectrometer bandpass filter. Either

---

*Kroutil, R.T., Research and Technology Directorate, U.S. Army Edgewood Research, Development and Engineering Center, August 1993, Unpublished data.

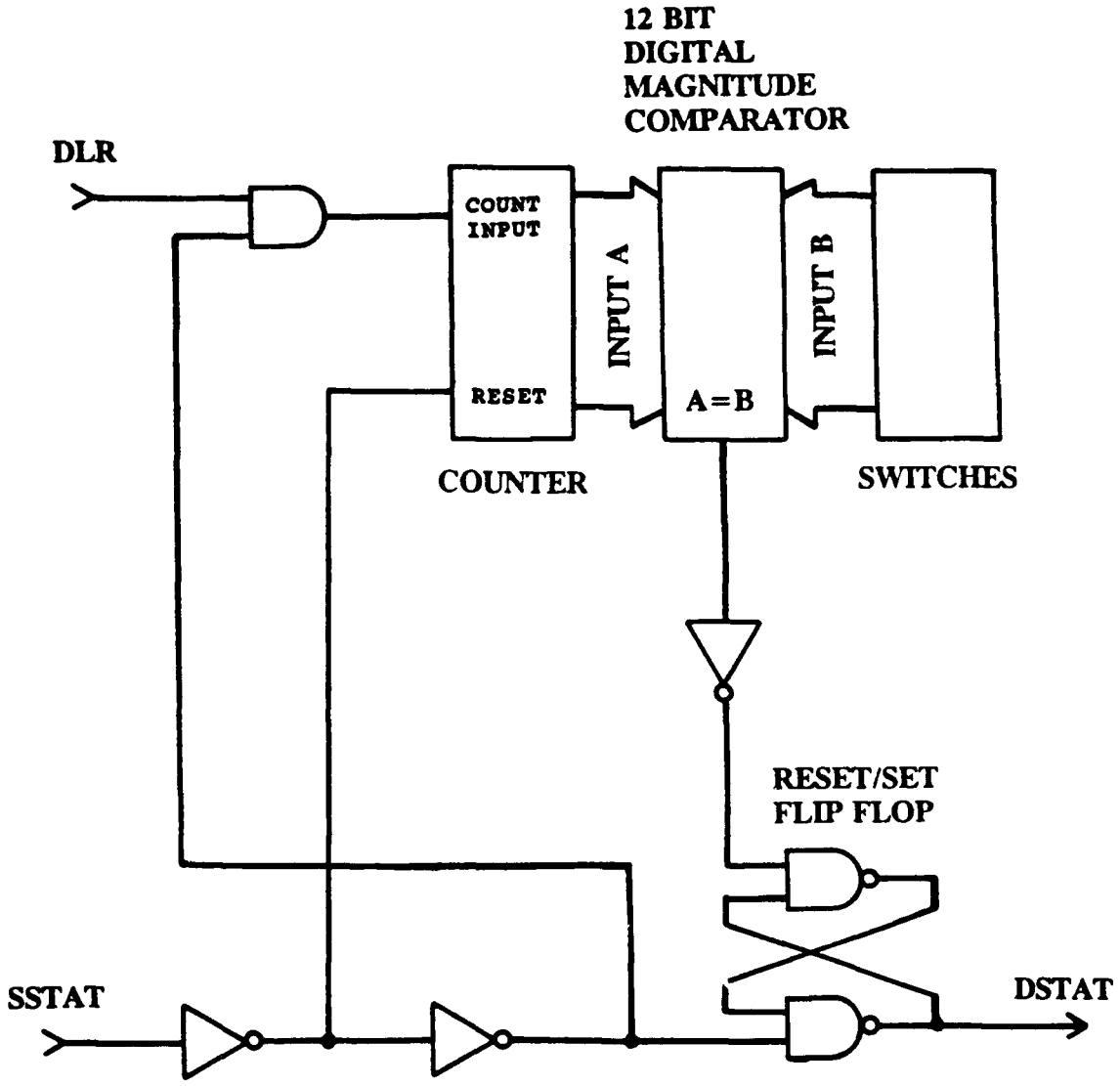

Figure 2. DSTAT Delay Interface Circuitry

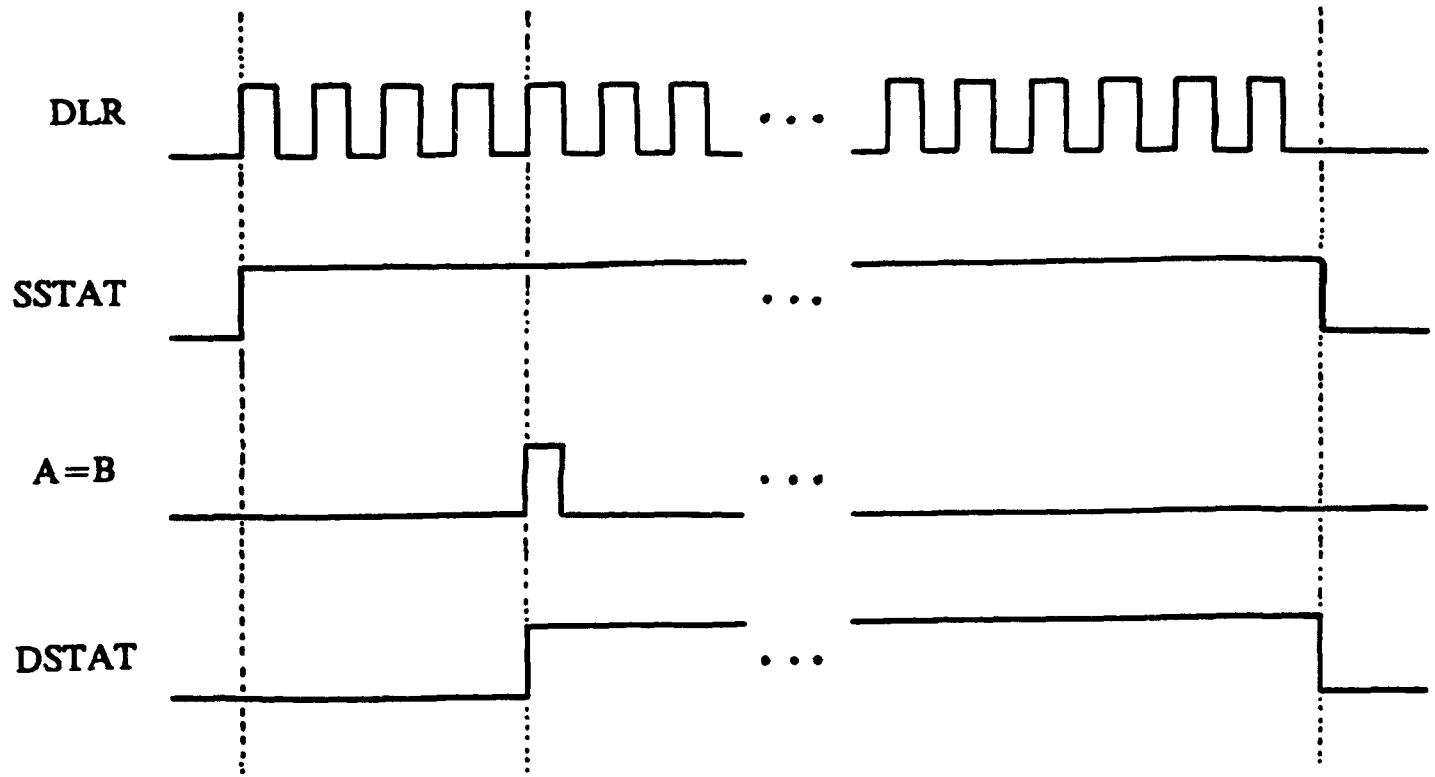

Figure 3. Timing Diagram for DSTAT Generation

the spectrometer SSTAT or DSTAT signal (for Case A or Case B, respectively) triggers the Analogic 2020 PWS sine wave generation. The PWS sine wave is subsequently sampled by the M2400-ZnSe spectrometer. For idealized Case C (i.e., synthetic mirror servo signals with no velocity errors), a monostable supplies the synchronizing SSTAT signal as shown in Figure 4. One Analogic 2020 PWS generates the simulated DLR signal, while another Analogic 2020 PWS provides the 1 V peak-to-peak, 500 Hz sine wave. These signals connect to the test points on the analog-to-digital conversion board with the mirror servo board cables disconnected.

The chopper modulation method employs an optical chopper with a 2 $in.^2$ aperture and 6 aperture blade. The EG&G Model 192 variable speed chopper modulates the IR radiation from an extended blackbody source at 500 Hz to the MIDAC spectrometer. The CI Systems SR-80 (CI Systems, Incorporated, Agoura Hills, CA) extended blackbody (i.e., 16 $in.^2$ in area) provides a NIST traceable IR radiation source accurate to within ± 0.03 °C and precise to ± 0.01 °C.[11] The SR-80 blackbody temperature of 50 °C furnishes a large contrast temperature to the ambient temperature chopper blade.

The MIDAC spectrometer is operated for at least 2 hr before collection of consecutive interferograms. This operation time permits thermal stabilization of the spectrometer. The spectrometer servo mirror control circuit determines the position of the zero OPD [i.e., zero optical path difference (ZPD) interferogram centerburst region]. Case A (large systematic mirror acceleration present) and Case B (small sinusoidal mirror velocity variation) represent a specific servo configuration. In both cases, the SR-80 extended blackbody (at 50 °C) provides a stable IR radiation source input during interferogram collection.[12] This interferogram collection includes the conditions necessary to determine the wavenumber axis accuracy with an ammonia spectrum. The ammonia spectrum is a difference spectrum. The difference spectrum is obtained from data collected with an ammonia and blank cell sequentially positioned between the SR-80 blackbody and MIDAC spectrometer. The short path gas cell provides a pathlength of approximately 82 mm.[13]

3. RESULTS

Spatial interferogram sampling along evenly divided increments in the OPD scale equals temporal interferogram sampling along uniform time intervals for a constant mirror velocity. Fluctuations from a constant mirror velocity results in a deviation from the uniform time intervals. Therefore, each method for measurement of the interferometer mirror velocity

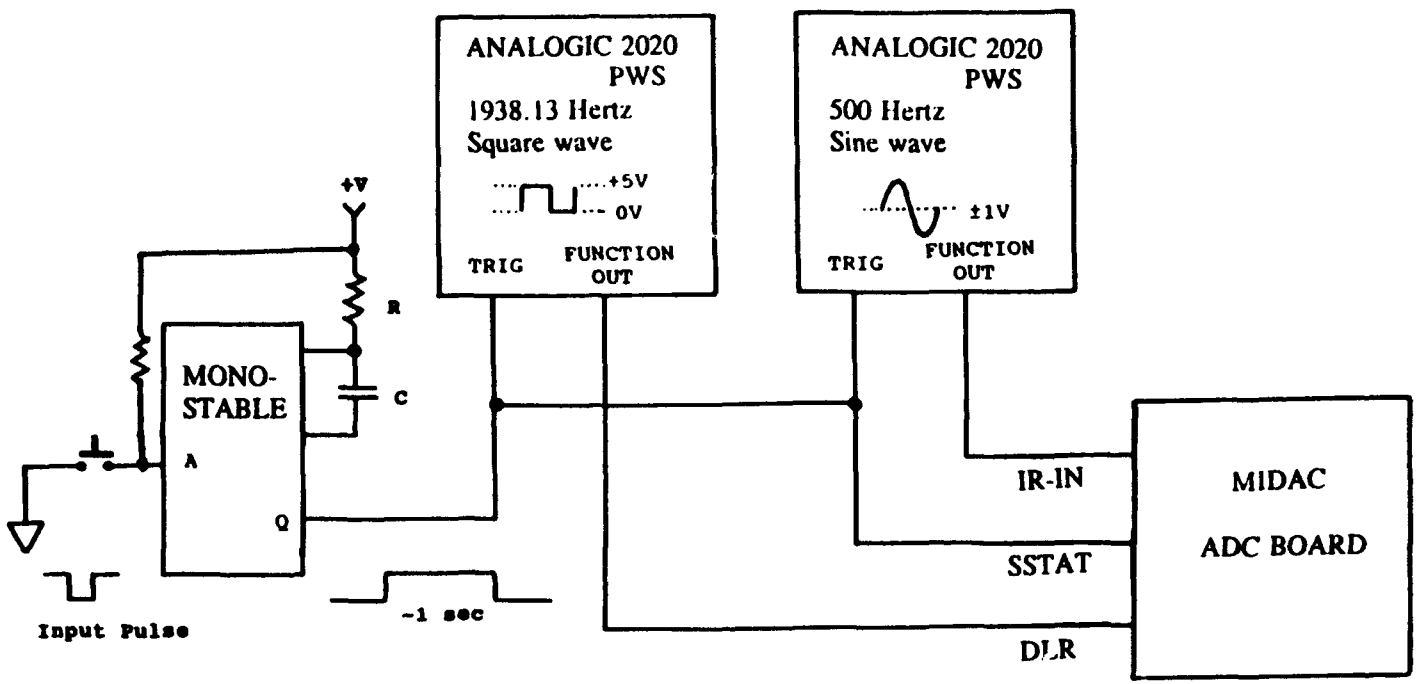

Figure 4. Synthetic Servo Mirror Signals Without Velocity Sampling Errors

employs some type of time measure (i.e., clock). The TIA method uses an approximately 68 MHz quartz oscillator time base to determine the time duration between interferogram sampling points. The sine wave test applies a known sinusoidal to the IR-input signal channel of the spectrometer. The 25 MHz time base for the Analogic 2020 PWS provides the sinusoidal input. The chopper modulation method produces an optical variation that is proportional to the chopper blade rotational speed. Examination of consecutive interferograms relies on the internal HeNe laser reference signal providing an accurate and precise interferogram sampling. The following presents the results for each of these four methods. Each method considers two cases: Case A, a systematic mirror acceleration due to mirror turn around is present and Case B, only a small sinusoidal variation in mirror velocity exists.

The TIA measurement results for Cases A and B are recorded in Table 1. The eight consecutive trials for each case show an average count value in column two (see Table 1) that gives a consistent scan-to-scan repeatability. Deviations (i.e., the best estimate of the standard error, ±BESE) from the average count value for Case A are approximately ±10%, while for Case B about ±0.2%. In Figure 5 the residuals for a single mirror scan are plotted for Cases A and B. The peak-to-peak variation of the DLR signal for Case A (see Figure 5) is approximately 60%. The mirror acceleration in Case A is revealed as a series of longer than average time interval counts that eventually converge to a constant value after about 800 time intervals. The peak-to-peak variation of the DLR signal for Case B (see Figure 6) is sinusoidal and approximately 1% in magnitude. The distribution of the time interval counts for Cases A and B (residuals shown in Figure 4) are plotted in Figure 7. The large skew in the distribution for Case A (see Figure 7) demonstrates the effect of a large mirror acceleration at mirror turn around. Only the first portion of the distribution for Case A is plotted in Figure 7. The maximum time interval count value for Case A is 27950. The average time interval count of 18326 falls a significant distance from the cluster of values near 17500. The deviation error of ±1754 from Table 1 encompasses values lower than 17428 that are not part of the Case A distribution range. The distribution for Case B (see Figure 8), with a range of time interval counts only 1/75th that of Case A, reflects the more stable maintenance of a constant mirror velocity. The average time interval count of 17464 for Case B occurs near the center of the distribution range in Figure 8. The deviation error of ±29 for Case B is included in the range of distribution values. For Case A, the maximum number of time interval count occurrences is only about one half that of Case B. Thus, the number of occurr-ences in the time interval count distribution also underscores the effects of a large systematic mirror acceleration. Con-secutive time interval measurement trials in Figure 9 provide a gauge of the scan-to-scan repeatability (i.e., precision). Figure 9 presents a plot

of the time interval count error bars (i.e., ±BESE) across the OPD scale for eight sequential mirror scans that are listed in Table 1. Case A (see Figure 9) contains a systematic acceleration error along the OPD scale as seen previously in the residual plot of a single scan (see Figure 5). Case B (see Figure 10) exhibits the same sinusoidal behavior seen in Figure 6. Clearly, the precision of ~0.2% for Cases A and B compares well, but the ability to maintain a constant mirror velocity differs significantly.

Table 1. Time Interval Analysis Results

$$t\ (cm/s) = 0.5 \times [SI(cm)/(\overline{tic} * toc(s))]$$

t: mirror velocity, cm/s
SI: sampling interval, cm
(2 x 632.8(10^{-9}) m x 100 cm/m)
tic: average time interval counts
toc: period of oscillator clock, s
(67.7576(10^{6}) Hz → 14.76285 ns)

File No.	$\overline{tic}$ (counts)	t_a (cm/s)	$[(t_a - t_l)/t_a] \times 100$ (%)	$[(t_u - t_a)/t_a] \times 100$ (%)
Case A:				
1.	18326 ± 1754	0.234	8.97	10.7
2.	18325 ± 1752	0.234	8.97	10.7
3.	18324 ± 1748	0.234	8.97	10.7
4.	18327 ± 1756	0.234	8.97	10.7
5.	18327 ± 1760	0.234	8.97	10.7
6.	18325 ± 1752	0.234	8.97	10.7
7.	18326 ± 1757	0.234	8.97	10.7
8.	18323 ± 1743	0.234	8.55	10.7
Case B:				
1.	17464 ± 29	0.2454	0.17	0.16
2.	17464 ± 28	0.2454	0.16	0.16
3.	17464 ± 29	0.2454	0.17	0.16
4.	17464 ± 29	0.2454	0.17	0.16
5.	17464 ± 29	0.2454	0.17	0.16
6.	17464 ± 29	0.2454	0.17	0.16
7.	17464 ± 29	0.2454	0.17	0.16
8.	17464 ± 29	0.2454	0.17	0.16

t_a: average mirror velocity (cm/s)
t_l: lower mirror velocity, $t_{a\text{-BESE}}$
t_u: upper mirror velocity, $t_{a\text{+BESE}}$

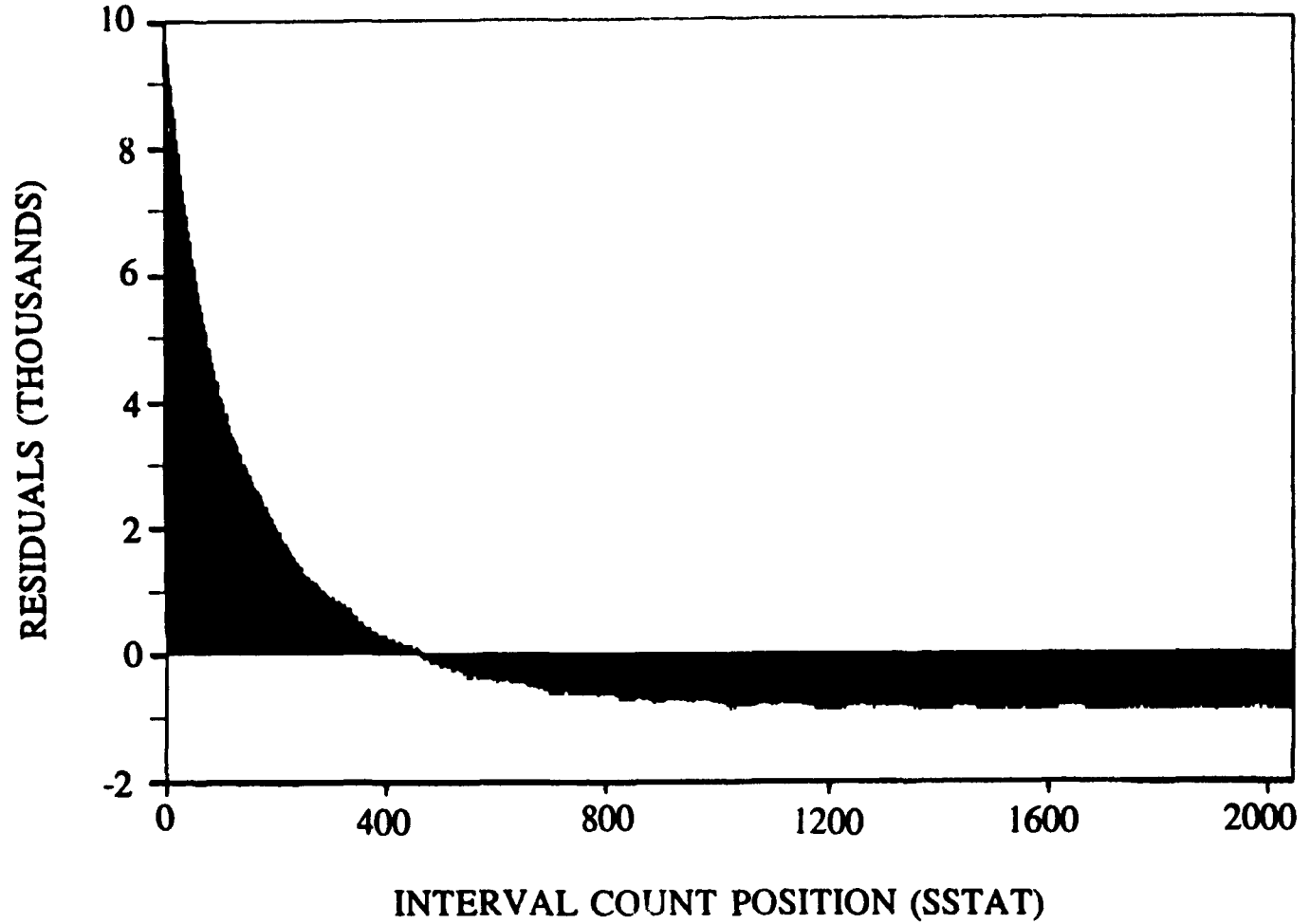

Figure 5. Variations of the Constant Velocity Sampling for Case A Servo Configuration

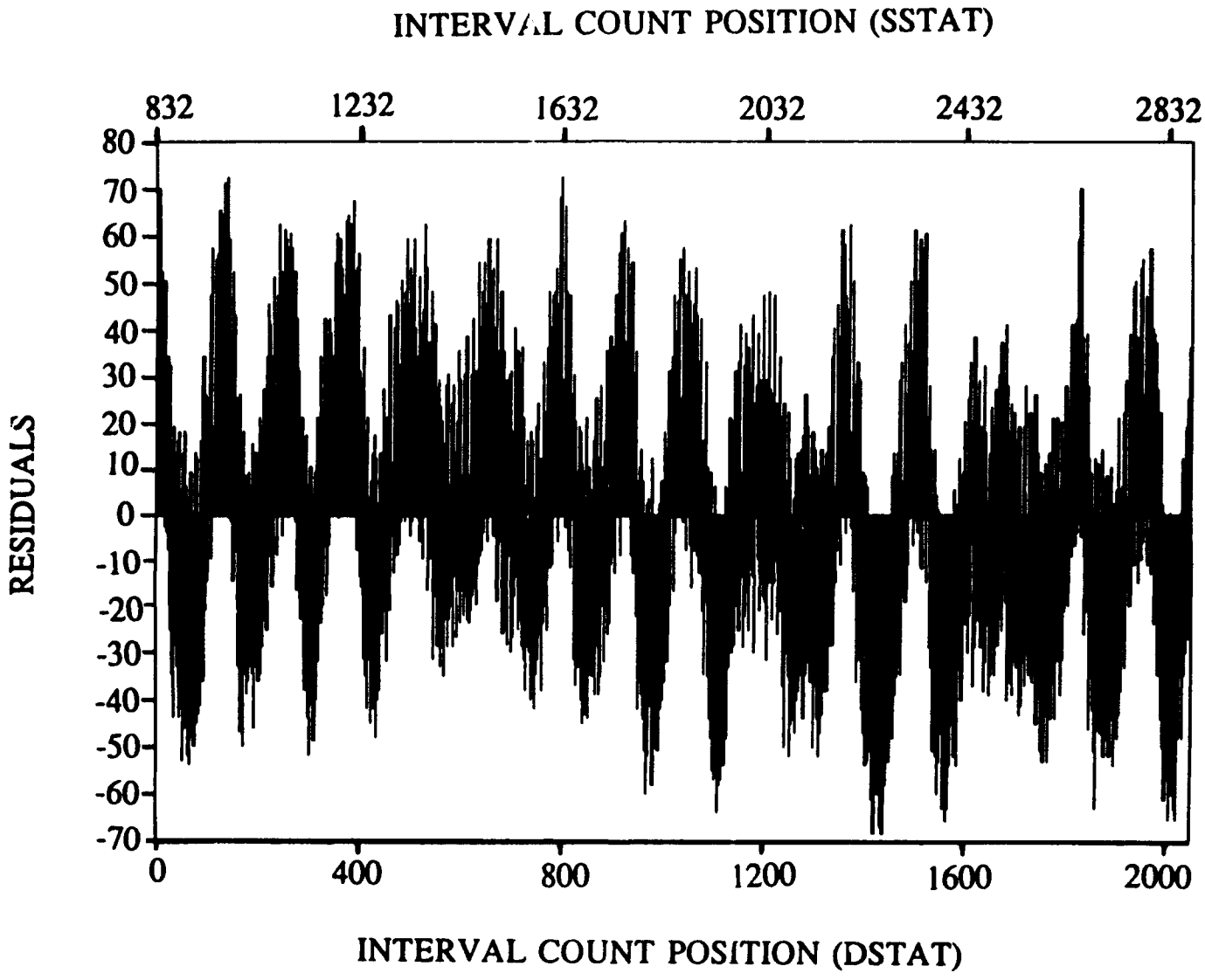

Figure 6. Variations of the Constant Velocity Sampling for Case B Servo Configuration

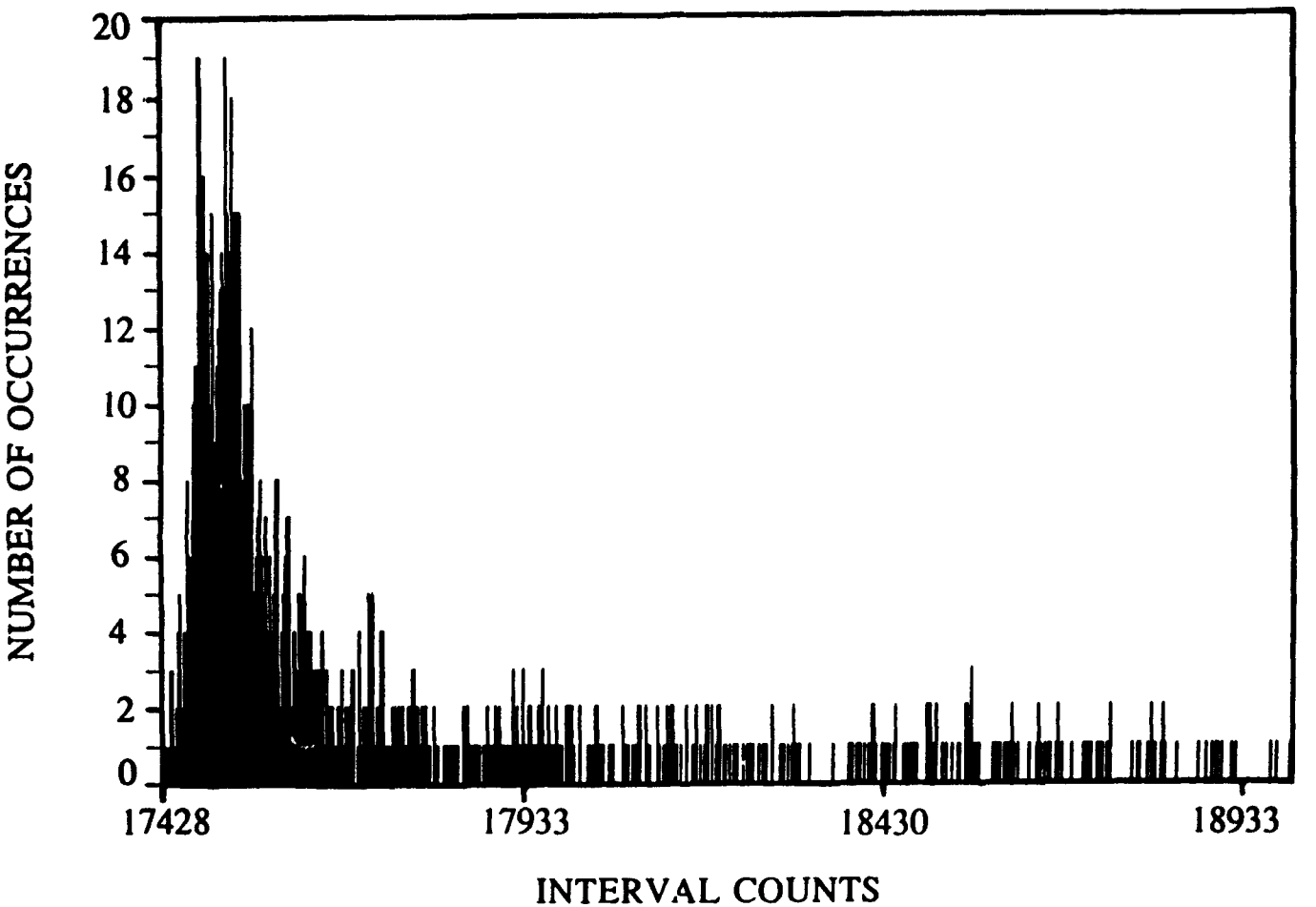

Figure 7. Distribution of Time Interval Counts for Case A Servo Configuration

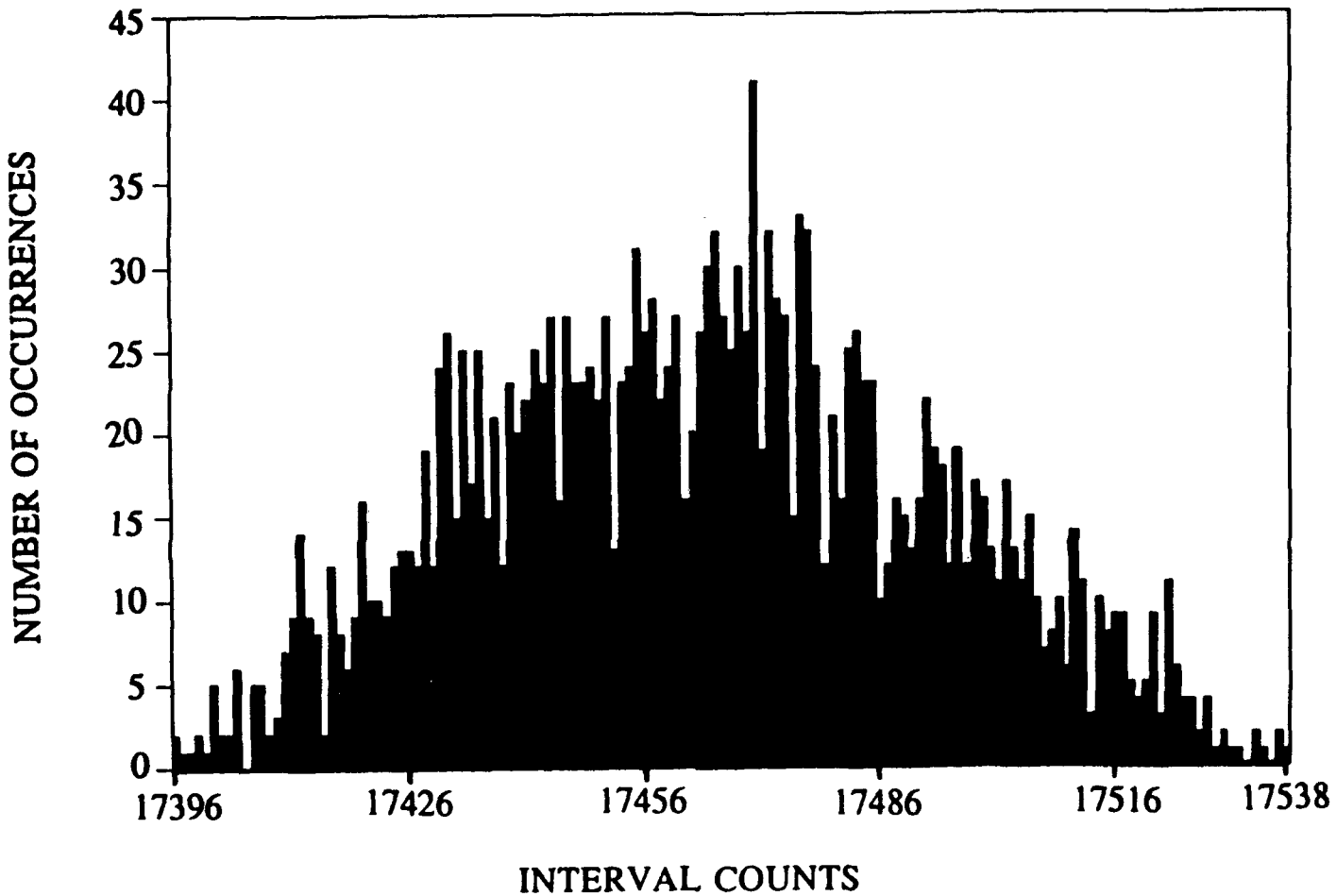

Figure 8. Distribution of Time Interval Counts for Case B Servo Configuration

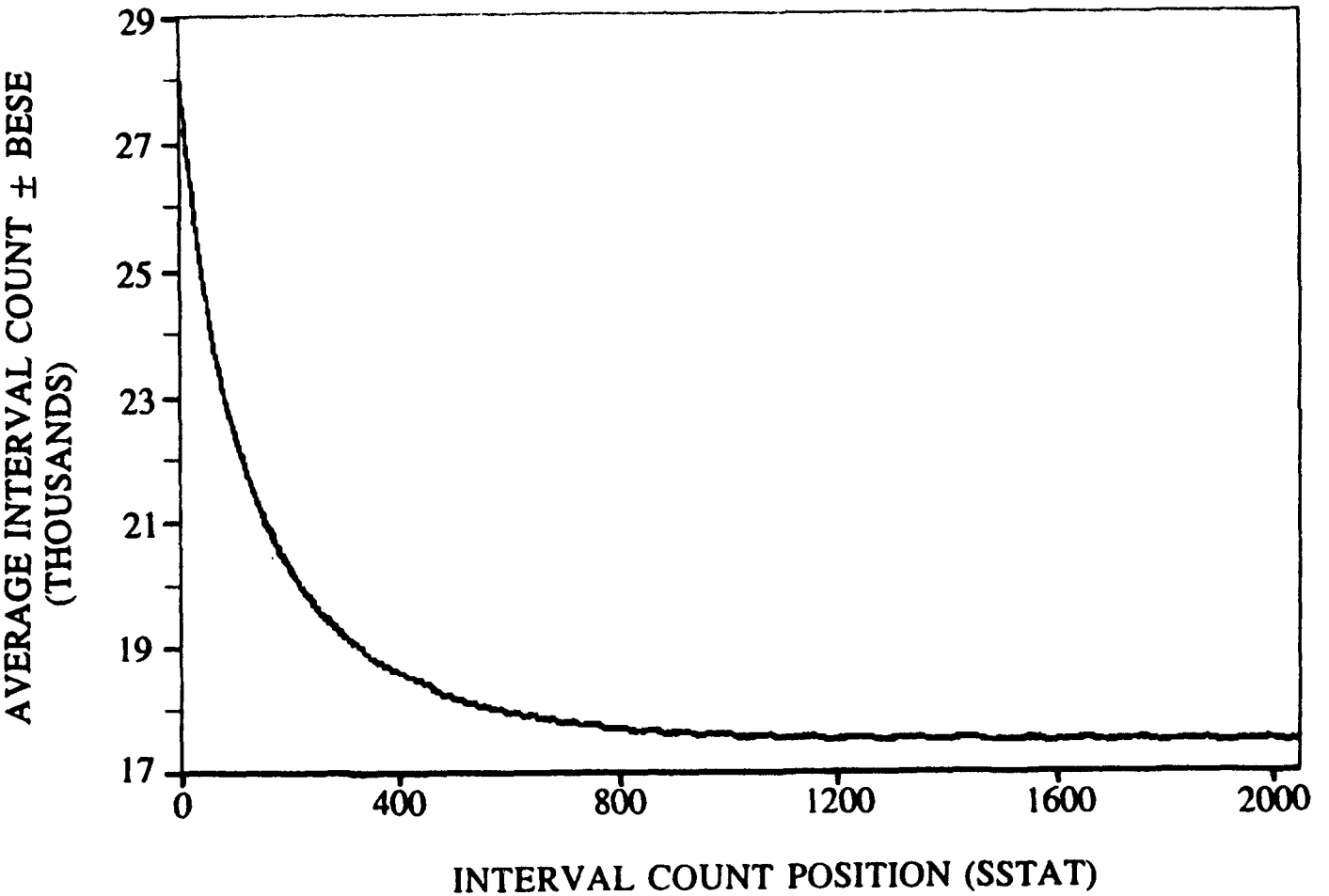

Figure 9. Scan-to-Scan Precision of Time Interval Counts for Case A Servo Configuration

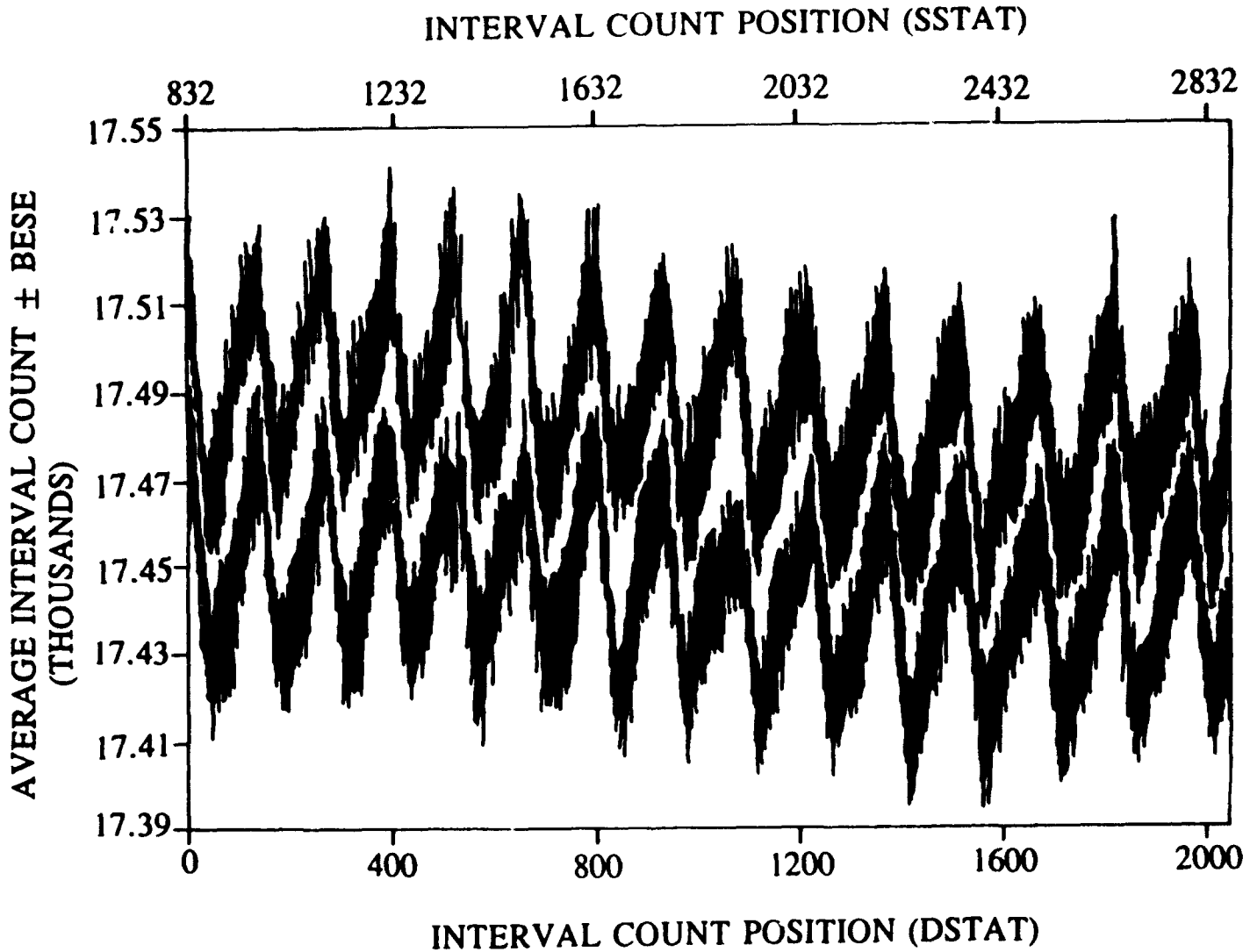

Figure 10. Scan-to-Scan Precision of Time Interval Counts for Case B Servo Configuration

The sine wave test results for Cases A and B are summarized in Figure 11 and Table 2. The spectra in Figure 11 are power spectra using triangular apodization and no phase correction. For a single frequency sine wave input, theoretically, the Dirac delta comb operator produces a single infinitely narrow frequency band. Practically, band distortion (i.e., spreading) occurs due to the limited spectral resolution, fluctuations in the servo mirror sampling, and characteristics of the bandpass filter.[2] The selected frequency of the input sine wave places the band position near the band pass filter center frequency. This selection minimizes band pass filter distortion. The three defining spectral band properties for the spectrometer response to the sine wave input are strength/amplitude, position/frequency, and width/coherence. Signal band strength for Case A is only about one third that of Case B. The band center of gravity positions[14] (i.e., CG) are comparable and differ by six wavenumbers. Bandwidths are calculated as full width at half height (FWHH) numbers. For Cases A and B, the FWHH differ by approximately a factor of six. The distortion of the bands for Case A results from the lower sampling rate around the interferogram centerburst region.

The optical chopper modulation results for Cases A and B are presented in Figure 12 and Table 2. The differential temperature between the 50 °C blackbody and ambient temperature chopper blade produces a waveform very similar in appearance to that of the sine wave test. The chopper modulation suppresses the interferogram centerburst region due to the modulation speed and large contrast in IR source temperatures. The fundamental frequency of the chopper modulation closely matches that used in the sine wave test. The same trends for band strength, position, and width are found for the chopper modulation (see Table 2). The major difference between the chopper modulation and sine wave test results lies in the base line variations (see Figure 11). Larger baseline fluctuations occur in the chopper modulation method. The detector response and chopper blade jitter contribute to these larger baseline fluctuations. The four satellite peaks in Case B (see Figure 12) are caused by the chopper blade jitter. These satellite peak magnitudes are 2 to 3% that of the major chopper modulation peak. Despite the baseline variations, the chopper results of Table 2 show band attenuation and distortion between Cases A and B, comparable to those seen in the sine wave test.

The collection of consecutive interferograms with a constant IR blackbody source filling the spectrometer field-of-view supplies a means to examine interferogram sampling precision. Figure 13 displays the co-addition of 100 interferograms near the interferogram centerburst region for Cases A and B. Figure 14 provides a plot of the deviation error (i.e., $\pm$BESE) for each sampled interferogram point near the centerburst

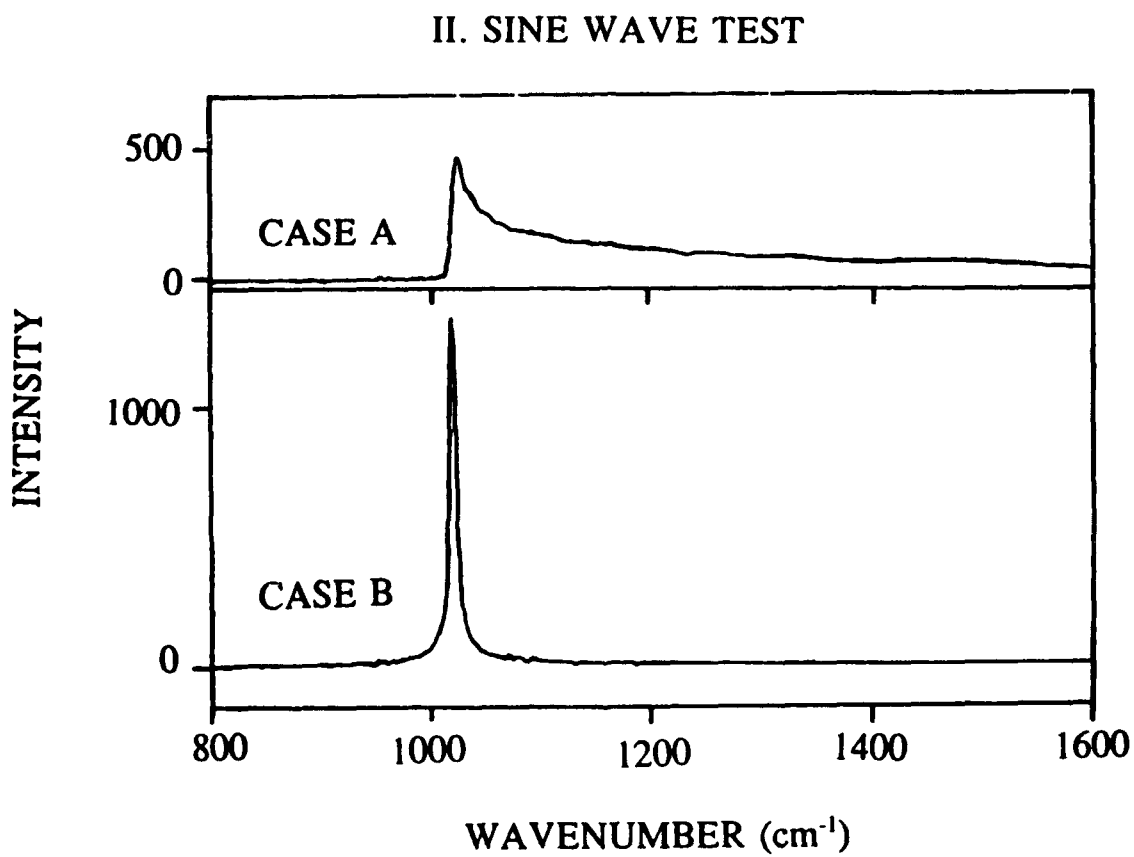

Figure 11. Sine Wave Test with 500 Hz, 1 V Peak-to-Peak Sine Wave for Cases A and B Servo Configuration

region for Cases A and B. The error deviations for Cases A and B are similar with a magnitude approximately 1% the averaged (note: 100 co-additions) interferogram signal. The oscillatory appearance in the error plots originates from the location of the sampled interferogram point. The deviation error in the sampled interferogram signal is greatest for a point sampled near a zero crossing (note: greatest slope) and least for a sampled value near a signal local minimum or maximum.[15] The deviation errors are not significantly different for the presence of mirror acceleration in Case A and the small sinusoidal mirror velocity variation in Case B.

Table 2. Comparison of Sine Wave Test and Chopper Modulation Results

Condition	Case	m_{CG} (cm^{-1})	Amplitude	FWHH (cm^{-1})
Sine Wave Test	A	1026	471	35
	B	1020	1351	6
Chopper Modulation	A	1027	1549	37
	B	1021	5000	6

The frequency domain spectra obtained from co-addition of 100 consecutive interferograms for Cases A and B show discernible differences in Figure 15. The magnitude of the difference between these co-added single beam spectrum (see Figure 16) is shown in Table 3 for select values across the active detector response region. Table 3 focuses only on variations for the range of detector response values of at least half the maximum detector response. The difference spectrum in Figure 16 between Cases A and B possesses an oscillatory behavior with definite wavelength dependence. The largest positive difference of 2.8% occurs at 917 cm^{-1} while the largest negative deviation of -7.9% appears at 1103 cm^{-1}. The percent errors are calculated with the Case B single beam spectrum. Clearly, the difference spectrum in Figure 16 and tabulated percentage errors in Table 3 illustrates the effects of a systematic mirror acceleration on spectrometer photometric accuracy. On the other hand, the precision associated with each averaged background (see Figure 17) shows insignificant differences across most of the active spectral region. The precision in Figure 18 is plotted as the percent error. The percentage is calculated with the absolute value of the BESE in the numerator and associated averaged spectrum in the denominator. It is interesting to note that the percent errors for Cases A and B do differ markedly in

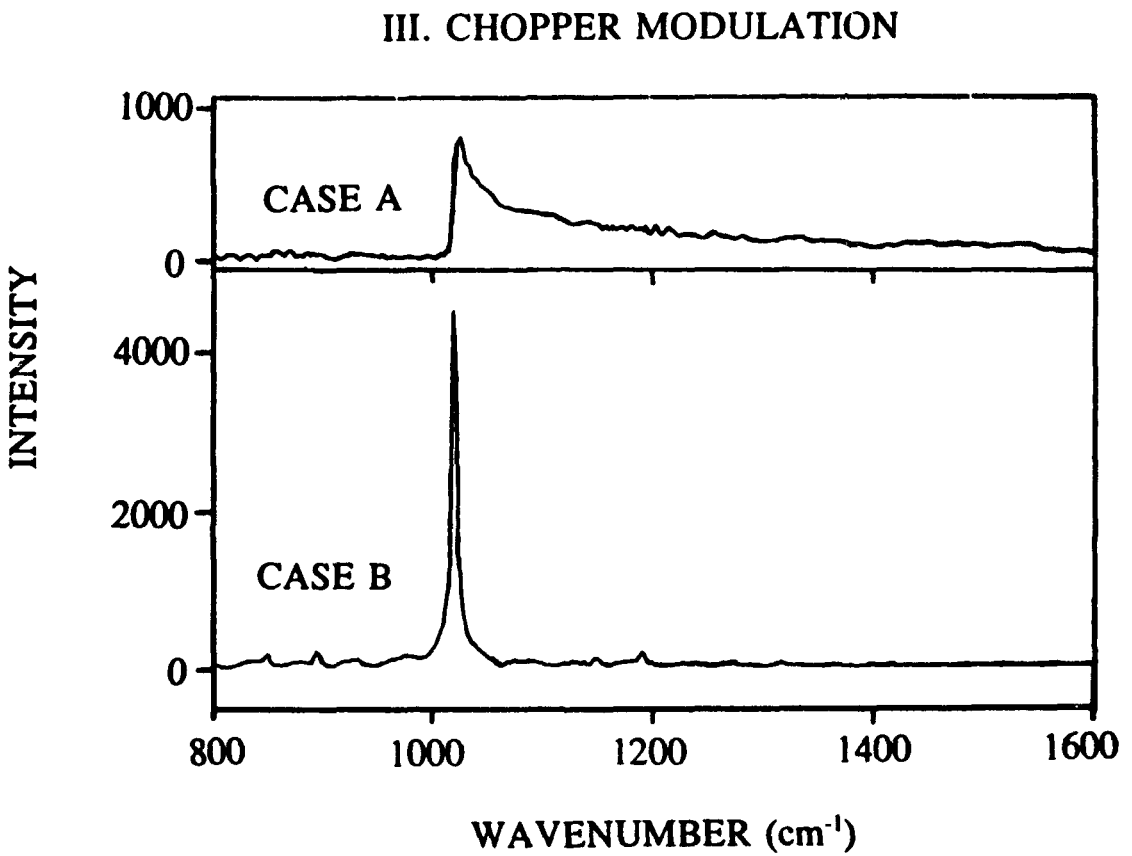

Figure 12. Chopper Modulation at 500 Hz of a 50 °C Blackbody for Cases A and B Servo Configuration

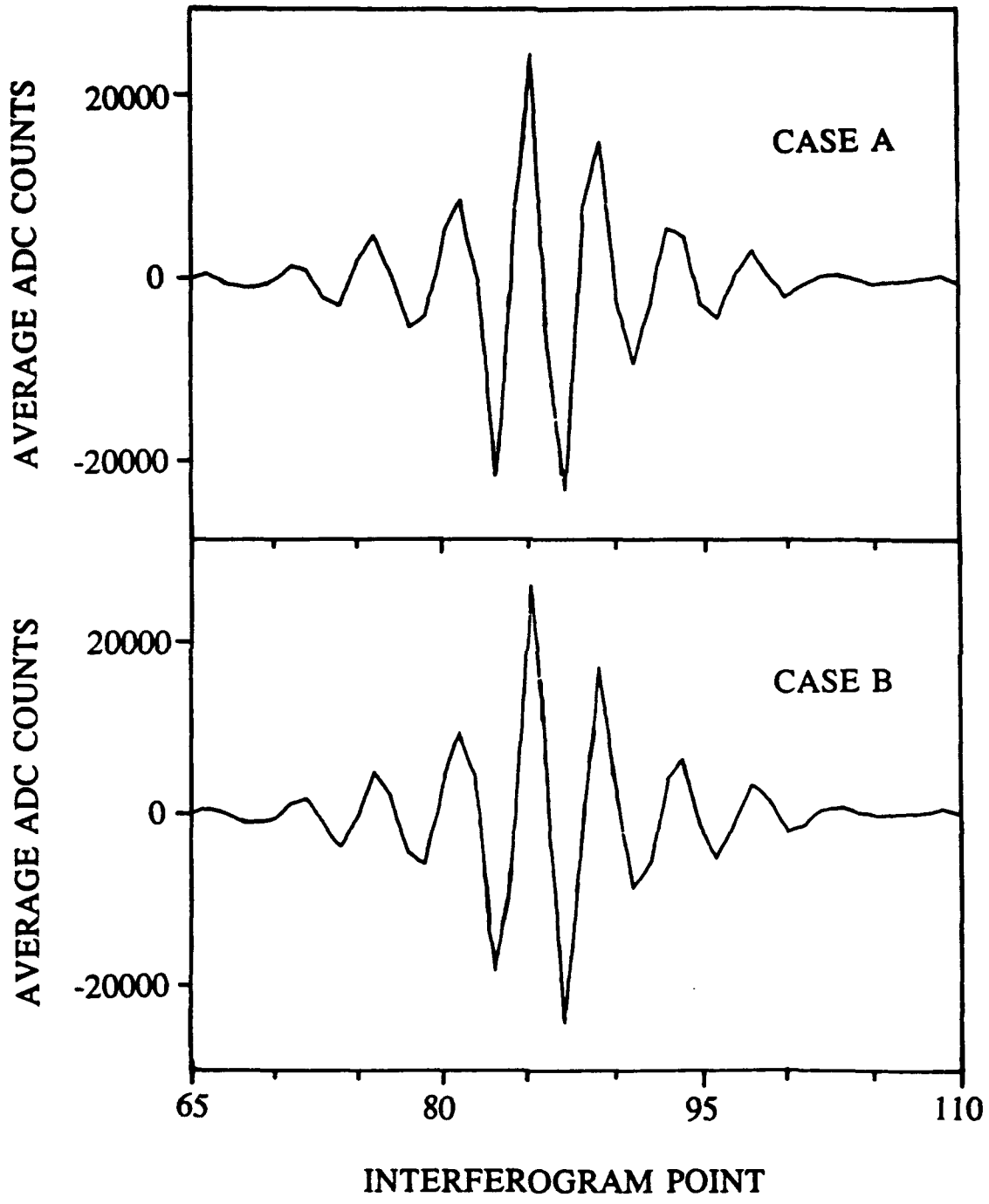

Figure 13. Centerburst Region for 100 Averaged Interferograms for Cases A and B Servo Configuration

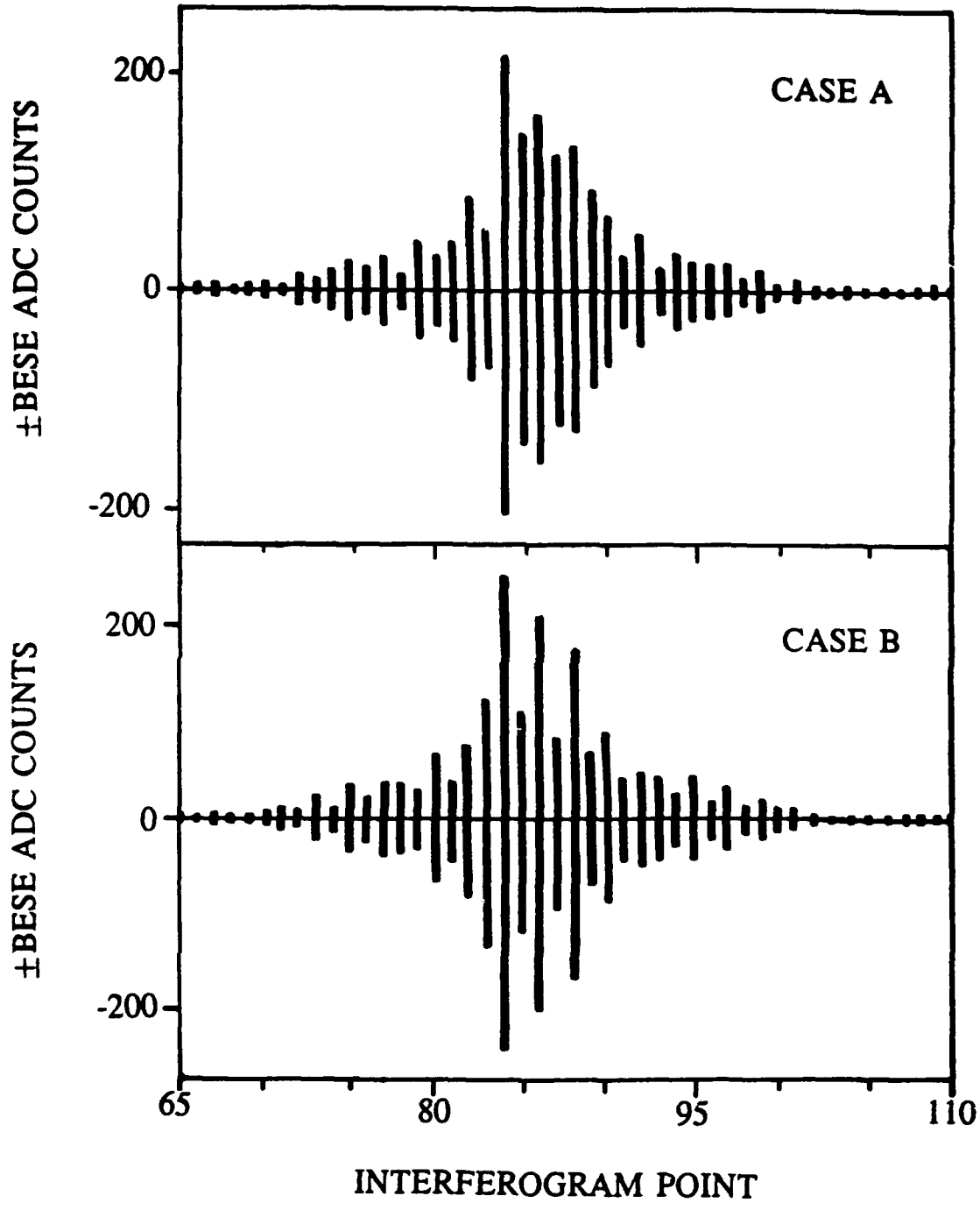

Figure 14. Errors Associated with 100 Averaged Interferograms for Cases A and B Servo Configurations in Centerburst Region

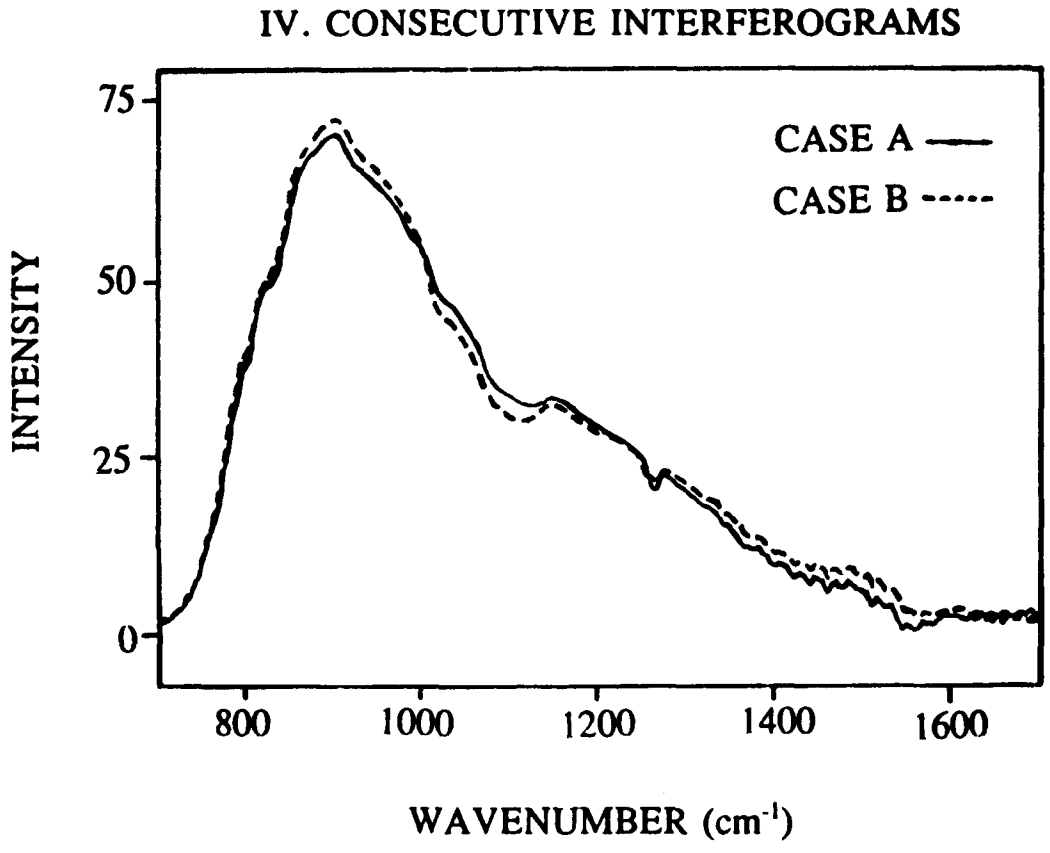

Figure 15. Comparison of Averaged Single-Beam Spectra for Cases A and B Servo Configuration

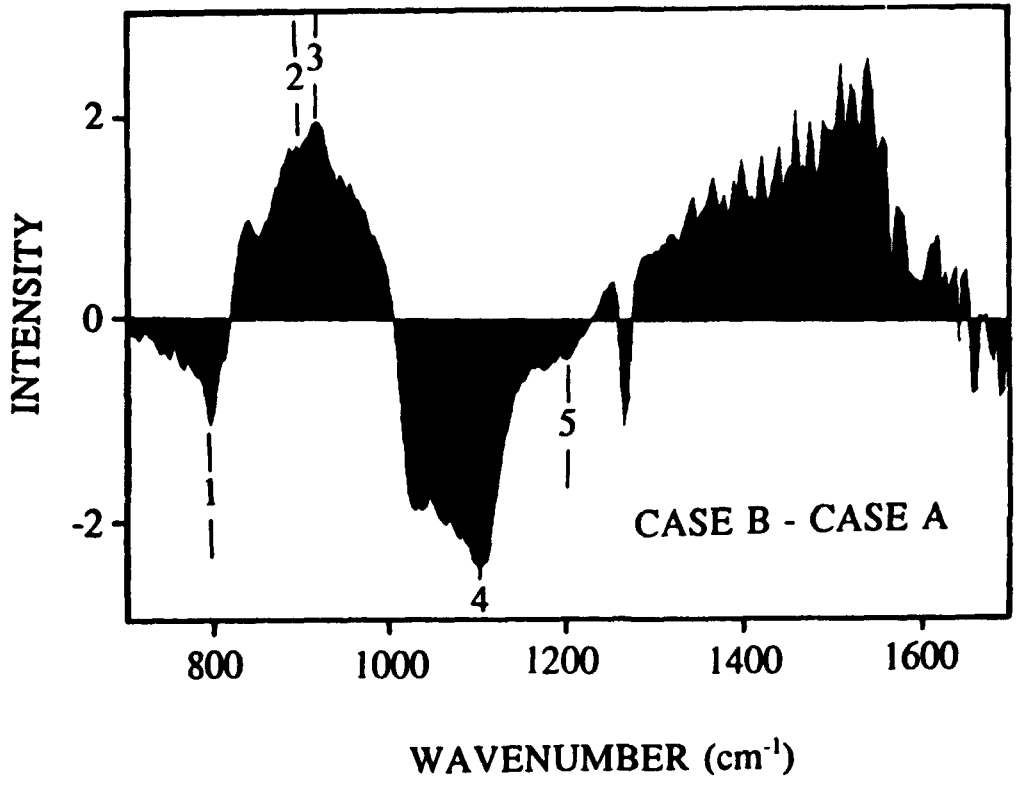

Figure 16. Difference Between Averaged Single-Beam Spectra for Cases A and B Servo Configuration

the 1550 cm^{-1} region (see Figure 17), where the detector response has fallen to <5% of the maximum.

Table 3. Percent Difference Between Detector Response for Cases A and B

	1	2	3	4	5
Percent Difference	-2.8	+2.4	+2.8	-7.9	-1.5
Wavenumber	797	901	917	1103	1200
Condition	½R	½R	D_{max}	D_{min}	½R

R: Single beam maximum response value
D: Difference maximum or minimum value

4. DISCUSSION

Modulation of the IR radiation by the Michelson interferometer is described by the following equation.

$$2 \cdot t \cdot m = f$$

The mirror velocity, t, has units of centimeters/second. The spectral band position, m, is in units of reciprocal centimeters. The modulation frequency, f, has units of Hertz.

Each of the four methods contribute known inputs to the interferometer modulation equation. The TIA measures time intervals associated with the DLR signal. These time intervals permit the calculation of the mirror velocity, t. The sine wave test and chopper modulation method supply a sinusoidal signal of known input frequency, f, and amplitude. Examination of consecutive interferograms using an ammonia gas sample (see Figure 19) furnishes a set of registration markers (i.e., documented spectral band positions), m.

The ammonia spectrum provides three documented[17] spectral line positions of 931.642 cm^{-1}, 949.656 cm^{-1}, and 968.122 cm^{-1}. Identification of these spectral features in the MIDAC spectrum are made. To determine the wavenumber axis registration on the MIDAC spectrum, the wavenumber axis is

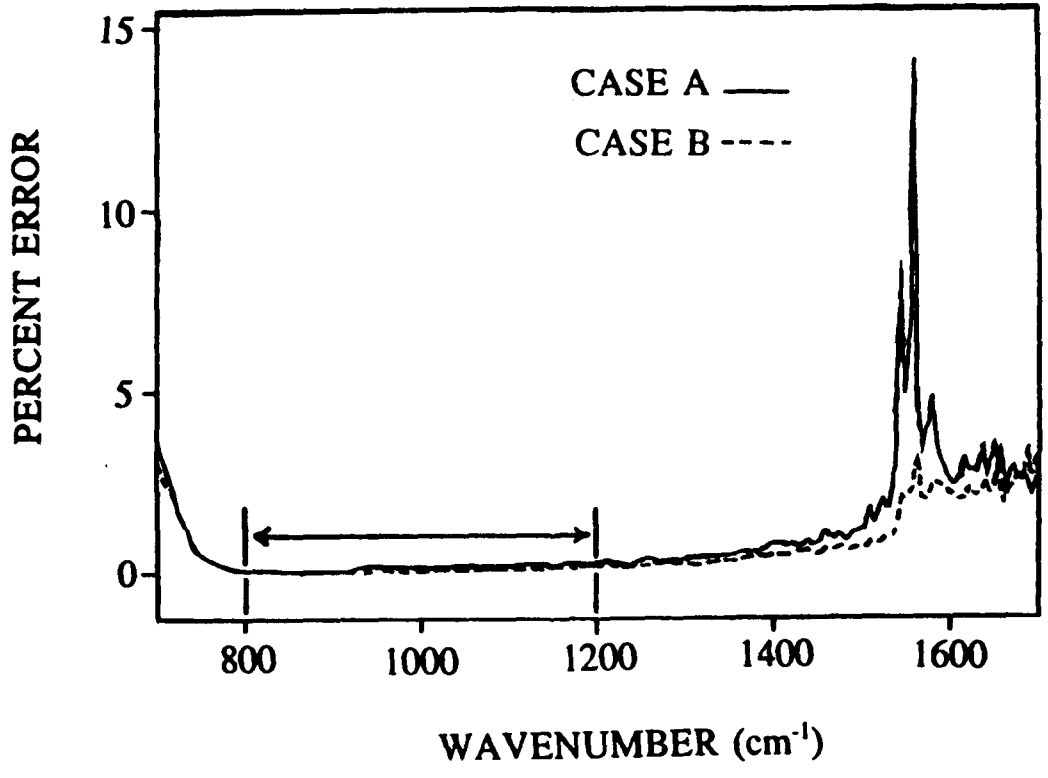

Figure 17. Comparison Spectral Precision from 700 to 1800 Wavenumbers for Cases A and B Servo Configuration

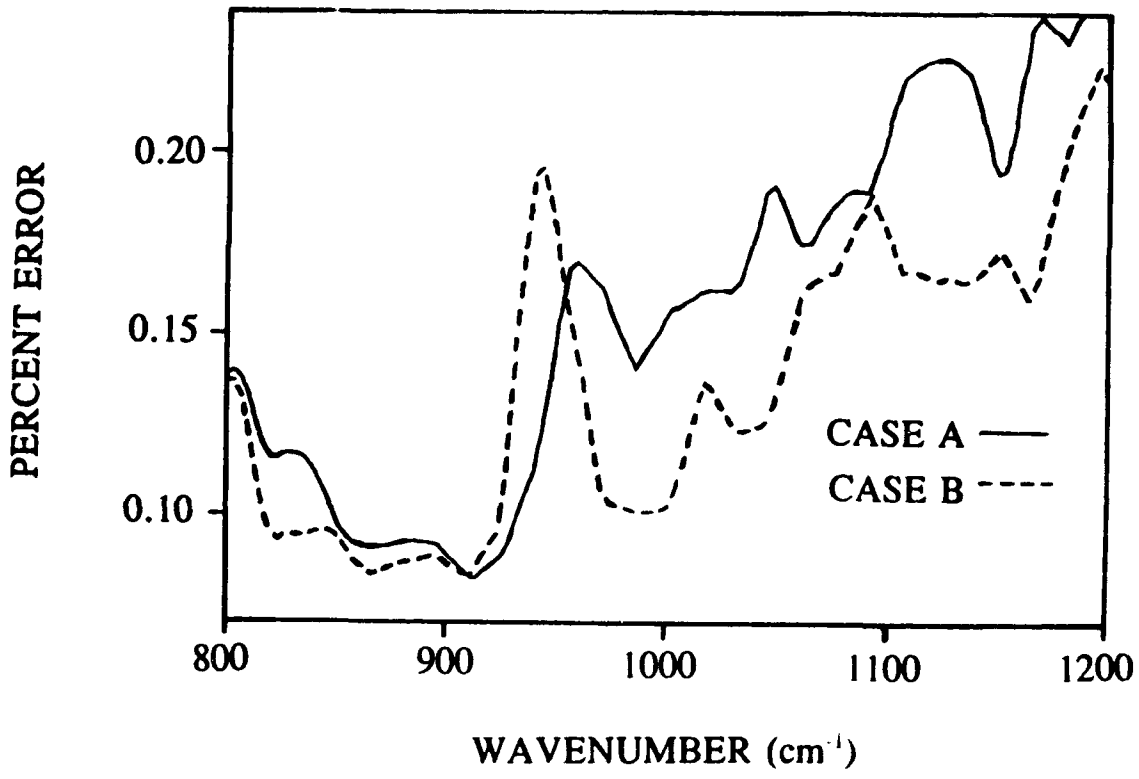

Figure 18. Comparison of Spectral Precision over Active Detector Response Region for Cases A ad B Servo Configuration

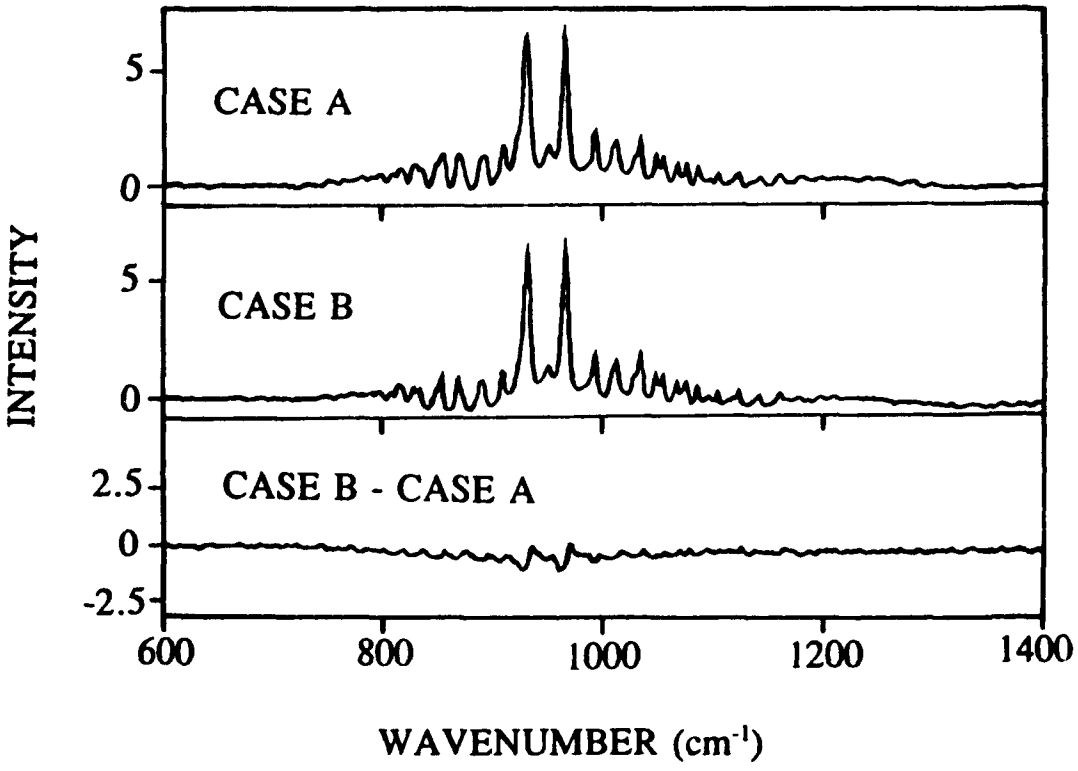

Figure 19. Ammonia Spectra for Cases A and B Servo Configuration

normalized by setting the lower and upper spectral values to zero and one, respectively. A plot of the literature spectral line positions[16] (abscissa) versus the MIDAC spectral positions (ordinate) is made. This selection of axes is based on the fact that the literature spectral positions are assumed to be the true values. A least squares line is calculated[17] that passes through the origin (i.e., zero intercept). The reciprocal of the least squares slope represents the maximum wavenumber value. For Cases A and B, the maximum wavenumber value is 1977.9 cm^{-1} and 1978.5 cm^{-1}, respectively. The maximum wavenumber value is one half the laser wavenumber typically input into the transform programs.[18] In this investigation, all wavenumber axes have been set to the Case B value for the comparison purposes. In Figure 19, the ammonia spectrum for Cases A and B are plotted along with the difference spectrum between Cases A and B. The most prominent spectral features at 931.6 cm^{-1} and 968.1 cm^{-1} differ between Cases A and B by approximately 10%. In spectroradiometric applications, the inherently small signal-to-noise values of spectral signatures make these small differences important.

The sine wave test permits the evaluation of systematic acceleration effects on known well characterized waveforms. A 500 Hz, 1 V peak-to-peak sine wave produces the results that are plotted in Figure 20. The spectra are obtained by fast Fourier transformation of the triangularly apodized waveform with a Mertz phase correction.[10] Note these plots differ markedly from the power spectra in Figure 7. This definitely shows that care must be exercised in the computational approach taken.[19] The plot of Case A with the large systematic mirror acceleration present in Figure 20 exhibits a large negative variation after the sine wave band. Also, the sine wave band for Case A has an amplitude only about one sixth that of either Case B (small mirror velocity variations) or Case C (no mirror velocity variations). The peak position of 1025.6 cm^{-1} for the small Case A band compares to the peak position of 1021.7 cm^{-1} for Cases B and C. Thus, the band in Case A becomes attenuated by about 84%, shifted by approximately 4 cm^{-1}, and distorted with ringing/broadening. On the other hand, Cases B and C are nearly identical with the difference being the absence of the small negative shoulder in Case C and very slight broadening in Case B. The sine wave band asymmetry in Case C may be due in part to band pass filter effects, because no mirror velocity sampling errors are present.

The sine wave test also permits evaluation of the effects of mirror velocity fluctuation on a damped sine wave. The damped sine wave provides a spectral signature of a specific band width. Selection of a Gaussian damping factor [i.e., $\exp(-x^2)$] allows consideration of the effects on a simulated broad band detector envelope and a simulated narrower band target signature.[20] Table 4 lists the equations input into the Analogic 2020 PWS necessary for generation of the damped sine wave curves.

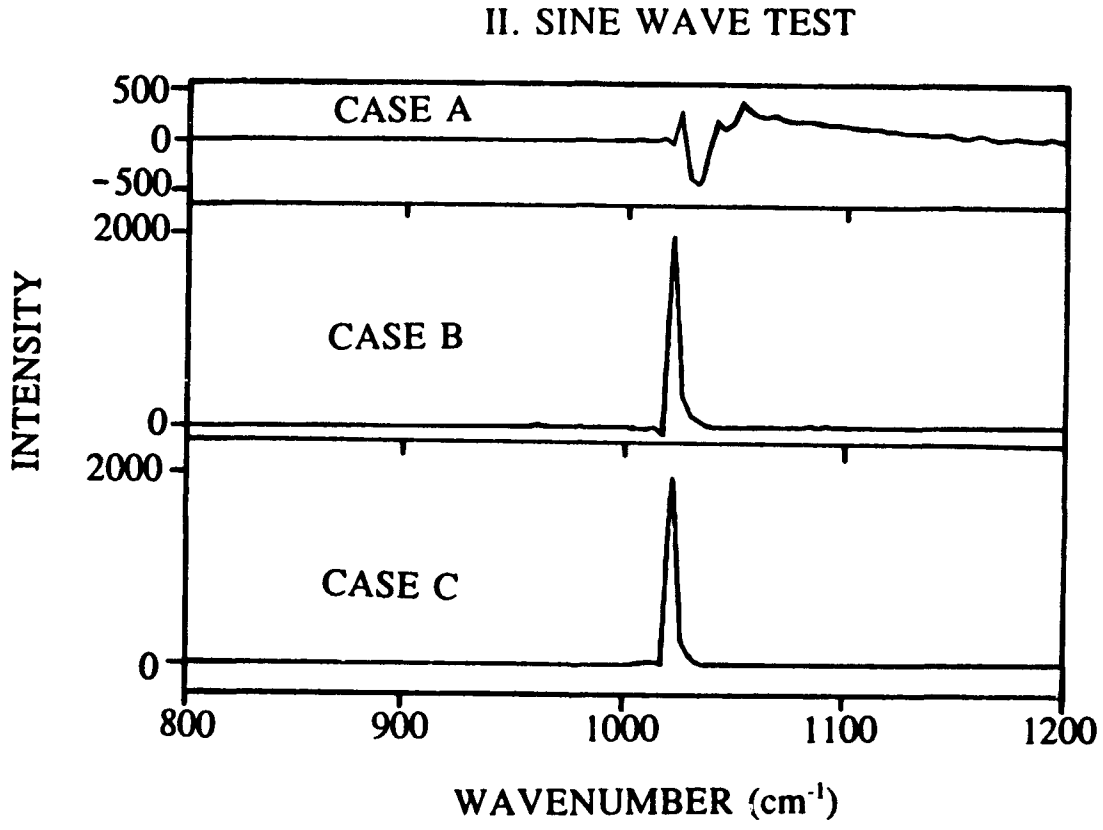

Figure 20. Sine wave Test Comparison of Three Cases: (A) Mirror Acceleration Present, (B) Small Sinusoidal Velocity Fluctuation, and (C) Constant Velocity

These curves are similar to those that are discussed in literature.[20] These damped sine waves are single-sided interferograms. The power spectra of the broadband envelope is shown in Figure 21. The difference power spectra between the broad and narrow bands is shown in Figure 22. Because these are single-sided interferograms, the damping of the sine wave begins upon receipt of the triggering signal (i.e., either the SSTAT or the DSTAT signal). This arrangement undoubtedly contributes to the large distortion and spectral shift that is seen for Case A (large mirror acceleration present). Case B, small sinusoidal mirror velocity variation, and Case C, no mirror velocity variation, are comparable. The pertinent spectral characteristics of the broadband and narrowband Gaussian curves of Figures 21 and 22 are summarized in Table 5. The broadband and narrowband responses for Cases B and C are quite similar with the center of mass position values for Cases B and C remaining within the spectrometer's resolution. For Case A, the band distortion shifts the center of mass position for the broadband signal 22 wavenumbers higher than the narrowband signal. This shift in Case A along with attenuation by about 10% of the maximum response as compared to Case C is consistent with previous results from the undamped sine wave test and ammonia registration measurements. Thus, the damped sine wave results demonstrate the effect of a large systematic acceleration error near the interferogram centerburst region. In summary, the damped sine wave input offers a sensitive measure of the mirror velocity effects on interferogram sampling.

Table 4. Analogic 2020 PWS Equations for Damped Sine Wave Generation

Broadband damped sine wave:

```
For 800m COS(440*t)/(e^((176*t)*(176*t))) CLK 15μ
```

Broadband - Narrowband damped sine wave:

```
For 800m -0.01*COS(440*t)/(e^(0.125*(32*t)*(32*t))) +
COS(440*t)/(e^((176*t)*(176*t))) CLK 15μ
```

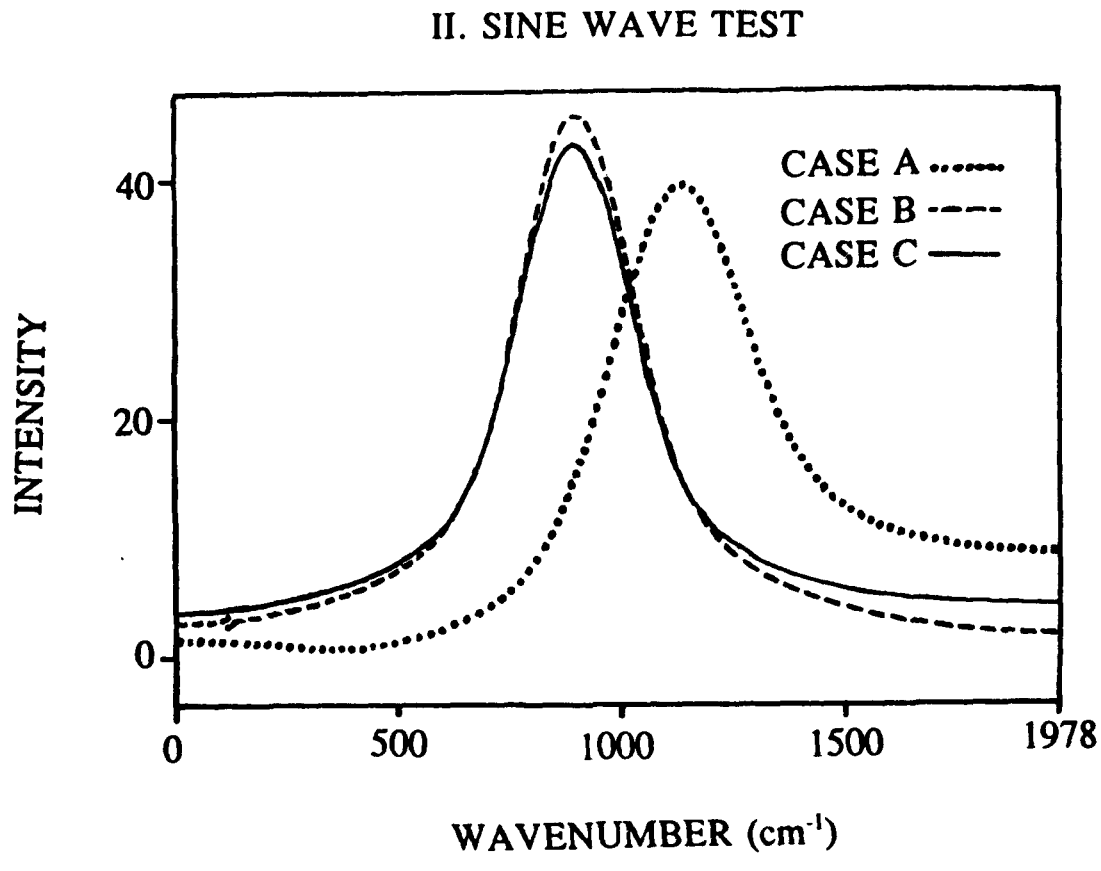

Figure 21. Damped Sine Wave Simulates Broadband Detector Response Envelope

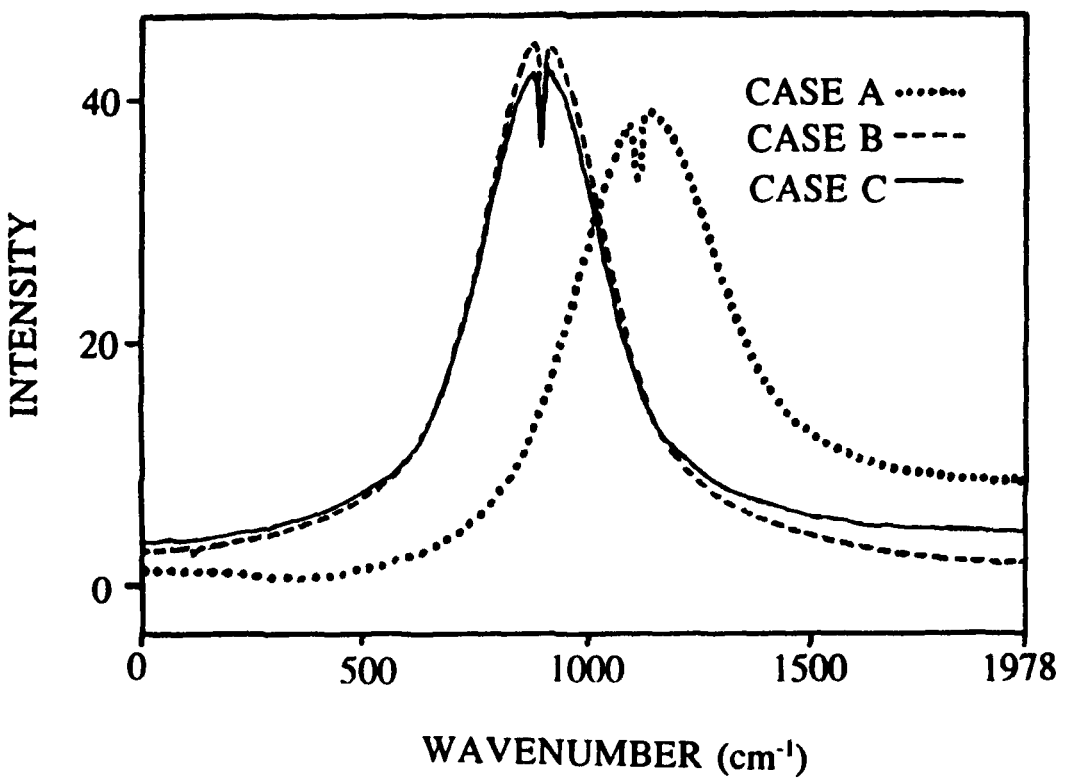

Figure 22. Idealized Narrowband Target Absorption Superimposed on Simulated Broadband Detector Response

Table 5. Damped Sine Wave Test Results

	Broadband		Narrowband	
	R_{max}	m_{CG} (cm^{-1})	D_{max}	m_{CG} (cm^{-1})
Case A	39.1	1136.3	5.4	1114.6
Case B	45.3	902.3	7.1	901.0
Case C	43.1	898.6	6.7	897.8

R_{max}: Maximum broadband response
D_{max}: Maximum narrowband response

5. CONCLUSIONS

Four evaluation methods permit the examination of mirror velocity variation effects on interferogram sampling. The time interval analysis (TIA) of the digitized laser reference (DLR) signal provides a direct measure of the mirror velocity and associated fluctuations. The sine wave test input of a known wavefor allows an evaluation of mirror velocity errors without an optical contribution from the infrared (IR) channel. The sine wave test using an undamped sine wave nearly identical to the frequency. The chopper modulation supplies an evaluation of the optical IR channel contributions. The final method, examination of consecutive interferograms, gives a measure of experimental precision. The examination of differences between consecutive interferograms or spectra alone does not detect the presence of systematic mirror accelerations. However, the use of all four methods in concert yields an evaluation of systematic and random errors associated with interferogram sampling. These interferogram sampling errors directly effect the performance of a Michelson interferometer as a spectroradiometer.

Blank

LITERATURE CITED

1. Zachor, A.S., "Drive Nonlinearities: Their Effects in Fourier Transform Spectroscopy," Applied Optics Vol. 16(5), pp 1412-1424 (1977).

2. Zachor, A.S., "Delay Compensation: Its Effect in Reducing Sampling Errors in Fourier Spectroscopy," Applied Optics Vol. 18(1), pp 68-75 (1979).

3. Piers, A., Poultney, S., and Logan, L.M., "Performance Models as Design Aids for Fourier Transform Spectrometers (FTS) Sensor System Developments," In Technologies of Cryogenically Cooled Sensors and Fourier Transform Spectrometers II," Proceedings of SPIE, Vol. 364, pp 21-29, The International Society for Optical Engineering, Billingham, WA, 1982, UNCLASSIFIED Report.

4. Logan, L.M., "Signal-to-noise Enhancement of Fourier Transform Spectroscopy (FTS) by Electrical Filter Compensation of Slide Velocity Errors," In "Multiplex and/or High-Throughput Spectroscopy," Proceedings of SPIE, Vol. 191, pp 110-113, The International Society for Optical Engineering, Billingham, WA, 1979, UNCLASSIFIED Report.

5. Combs, R.J., and Cathey, C.T., "Measurement of a Michelson Interferometer Mirror Velocity," Analytical Instrumentation Vol. 20(4), pp 223-256 (1992).

6. Saperstein, D.D., "The Sine Wave Test for Fourier Transform Infrared Spectrometers," Spectroscopy Vol. 2(8), pp 45-47 (1986).

7. deHaseth, J.A., "Stability of Rapid Scanning Interferometers," Applied Spectroscopy Vol. 36(5), pp 544-552 (1982).

8. Beer, R., "Remote Sensing by Fourier Transform Spectrometry," p 75 and pp 101-127, John Wiley & Sons, New York, NY, 1992.

9. Kuehl, D., "An Optimized Programming Language/ Environment for Processing Scientific Data," Spectroscopy Vol. 4(1), pp 30-34 (1989).

10. User Manual for Polynomial Waveform Synthesizer Model 2020, Analogic Corporation, Peabody, MA, 1990.

11. SR-80 Extended Area Infrared Radiation Source, Operation Manual, 550-490-0010, CI Systems Inc., Agoura Hills, CA, 1989.

12. van Kasteren, P.H.G., "Quantitative Aspects of FT-IR Spectroscopy in Industrial Applications," In Analytical Applications of FT-IR to Molecular and Biological Systems, J.R. Durig, Editor, Pub. D. Reidel, Dordrecht, Holland, 1980, pp 203-228.

13. Combs, R.J., and Knapp, R.B., "Response Time of a Short-Scan Interferometer for Stand-off Detection of Chemical Agents," CRDEC-TR-387, U.S. Army Chemical Research, Development and Engineering Directorate, Aberdeen Proving Ground, MD, July 1992, UNCLASSIFIED Report.

14. Cameron, D.G., Kauppinen, J.K., Moffact D.J., and Mantsch, H.N., "Precision in Condense Phase Vibrational Spectroscopy," Applied Spectroscopy Vol. 36(3), pp 245-250 (1982).

15. Bendat, J.S., and Piersol, A.G., "Engineering Applications of Correlation and Spectral Analysis, 2nd ed., pp 35-37, John Wiley & Sons, New York, NY, 1993.

16. Rothman, L.S., et al., "The HITRAN database: 1986 edition," Applied Optics Vol. 26(19), pp 4058-4097 (1987).

17. Field, P.E., PHYSICAL METHODS IN CHEMISTRY, pp 9-10 and pp 24-25, Virginia Polytechnical Institute and State University, Blacksburg, VA, 1979.

18. Griffiths, P.R., and deHaseth, J.A., "FOURIER TRANSFORM INFRARED SPECTROMETRY," In CHEMICAL ANALYSIS SERIES, Vol. 83, John Wiley & Sons, New York, NY, p 38, 1986.

19. Connes, J., "Recherches sur la Spectroscopie par Transformation de Fourier," Revue d'Optique Vol. 40, pp 45-78, 116-140, 171-190, and 231-265 (1961).

20. Small, G.W., Harms, A.C., Kroutil, R.T., Ditillo, J.T., and Loerop, W.L., "Design of Optimized Finite Impulse Response Digital Filters for use with Passive Fourier Transform Infrared Interferograms," Analytical Chemistry Vol. 62(17), pp 1768-1777 (1990).